

# Saturation field of frustrated chain cuprates: broad regions of predominant interchain coupling

S. Nishimoto,<sup>1</sup> S.-L. Drechsler\*,<sup>1</sup> R.O. Kuzian,<sup>1</sup> J. van den Brink,<sup>1</sup>  
J. Richter,<sup>2</sup> W.E.A. Lorenz,<sup>1</sup> Y. Skourski,<sup>3</sup> R. Klingeler,<sup>4</sup> and B. Büchner<sup>1</sup>

<sup>1</sup>IFW Dresden, P.O. Box 270116, D-01171 Dresden, Germany

<sup>2</sup>Universität Magdeburg, Institut für Theoretische Physik, Germany

<sup>3</sup>Hochfeld-Magnetlabor Dresden, Helmholtz-Zentrum Dresden-Rossendorf, D-01314 Dresden, Germany

<sup>4</sup>Kirchhoff Institute for Physics, University of Heidelberg, D-69120 Heidelberg, Germany

(Dated: November 12, 2018)

An efficient and precise thermodynamic method to extract the interchain coupling (IC) of spatially anisotropic 2D or 3D spin-1/2 systems from their empirical saturation field  $H_s$  ( $T = 0$ ) is proposed. Using density-matrix renormalization group, hard-core boson, and spin-wave theory we study how  $H_s$  is affected by an antiferromagnetic (AFM) IC between frustrated chains described in the  $J_1$ - $J_2$ -spin model with ferromagnetic 1st and AFM 2nd neighbor inchain exchange. A complex 3D-phase diagram has been found. For  $\text{Li}_2\text{CuO}_2$  and  $\text{Ca}_2\text{Y}_2\text{Cu}_5\text{O}_{10}$ , we show that  $H_s$  is solely determined by the IC and predict  $H_s \approx 61$  T for the latter. Using  $H_s \approx 55$  T from our high-field pulsed measurements one reads out a weak IC for  $\text{Li}_2\text{CuO}_2$  close to that from neutron scattering.

Since real spin chain systems exhibit besides a significant in-chain coupling also an *interchain* coupling (IC), one may ask: in which cases is this relatively weak IC still important or even crucial? From the Mermin-Wagner theorem its decisive role for the suppression of fluctuations is well-known. The IC leads to magnetic long-range order (LRO) at  $T = 0$  in 2D [1] and at  $T < T_N$  in 3D (see e.g. Ref. 2). Often one is faced with a situation that the (large) in-chain couplings are known with reasonable precision, e.g. from band-structure calculations, inelastic neutron scattering (INS) or susceptibility data [3], but precise values for the tiny (nevertheless important) IC are lacking. If frustration is absent, the IC can be determined quite accurately, e.g. from  $T_N$  analyzed by Quantum Monte Carlo based studies [4] and more approximately using mean-field theory for a 3D IC [5]. But how to extract from experimental data a small IC for frustrated systems with weakly coupled chains where these methods do not work? Here we address such a 2D/3D problem for the case of frustrated spin-1/2 chains with ferromagnetic (FM) nearest-neighbor and antiferromagnetic (AFM) next-nearest-neighbor exchange described by the spin isotropic  $J_1$ - $J_2$ -model (IM). Nowadays it is the standard model for edge-shared chain cuprates (see e.g. [6]). This 1D-IM attracted special interest [8–13] due to a rich phase diagram with multipolar (MP) phases derived from multi-magnon bound states (MBS) in high magnetic fields [14–16]. Additional AFM degrees of freedom enhance the kinetic energy of magnons. Thus, AFM IC might disfavor multi-MBS. A precise knowledge of the magnitude of the IC is therefore a necessary prerequisite to attack the multi-MBS problem, including a possible MBS Bose-Einstein condensation. Hence, knowing it is of general interest [17–20].

In this context,  $\text{Li}_2\text{CuO}_2$  (see Fig. 1) is one of the best studied frustrated cuprates and therefore well suited to compare theory and experiment. In particular,

using spin-wave theory (SWT) the main in-chain and IC  $J$ 's were extracted from INS data and a specific AFM IC was found crucial for preventing spiral order in the 3D ground state (GS) [3]. If the saturation field  $H_s$  can be determined experimentally, an excellent opportunity occurs to check the INS based IC. But for  $\text{Li}_2\text{CuO}_2$   $H_s$  has not been measured so far. Here we report high-field magnetization data to fill this gap. Our paper is organized as follows. First we revisit the 1D case and provide details of the density-matrix renormalization group (DMRG) technique involved. Then we report results for coupled chains, among them a rather complex phase diagram, and compare our findings with our experimental  $H_s$ -data for  $\text{Li}_2\text{CuO}_2$  and arrive at an almost perfect explanation in terms of a predominant IC.

We apply the DMRG method [21] with periodic boundary conditions (PBC) in all directions. Seemingly, this method is much less favorable for  $D > 1$ ; however, on current workstations using highly efficient DMRG codes, spin systems with up to about  $\sqrt{10} \times \sqrt{10} \times 50$  sites, i.e. 10 coupled chains of length  $L \sim 50$ , can be studied.

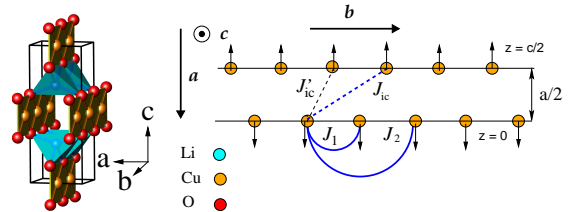


FIG. 1: (Color) Left: Crystal structure of  $\text{Li}_2\text{CuO}_2$  with two  $\text{CuO}_2$  chains per unit cell along the  $b$ -axis. Right: View along the  $c$ -axis on the  $ab$ -plane. The main in- and interchain couplings  $J_{1,2}$  and  $J_{ic}$ ,  $J'_{ic}$ : arcs and dashed lines, respectively. The normalized ICs read  $\beta_1 = J'_{ic}/|J_1|$  and  $\beta_2 = J_{ic}/|J_1|$ .

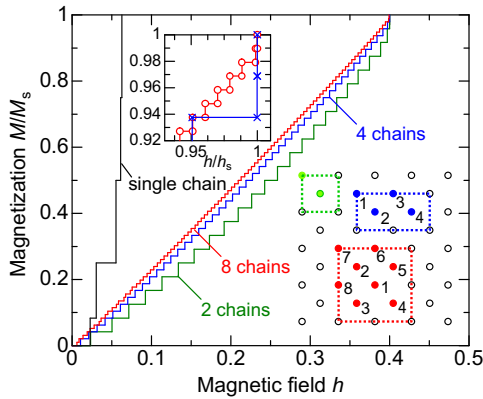


FIG. 2: (Color) Magnetization vs. external field (DMRG data) for different  $n$  as shown in the inset, for  $\alpha = J_2/|J_1| = 1/3$ ,  $\beta_2 = 0.05$ ,  $\beta_1 = 0$ , and  $L = 24$  sites in each chain. Lower inset: The 3D arrangement of chains used for the DMRG study reported here. Upper inset: Magnetization curve inside the 3-MBS region for  $\beta_2 = 0.005$  (blue curve,  $\times$ ) compared with that for the 1-magnon C-phase for  $\beta_2 = 0.05$  (red curve,  $\circ$ ). Note the three times larger step for  $\beta_2 = 0.005$ .

Thus, by taking a proper arrangement of the chains 3D lattices can be simulated, cf. the inset in Fig. 2. Let us now describe how the block states are constructed: in the  $n \times L$  cluster, where  $n$  denotes the number of chains and  $L$  is the chain length. If we regard  $n$  sites in the  $ac$ -plane as a “unit cell”, the system can be treated as an effective 1D chain with  $L$  sites (step 1). This enables us to use an appropriate 1D array for the construction of the PBC (see Fig. 1 of Ref. 22). In the second step the sites within each “unit cell” are arranged into numeric order as shown in the inset of Fig. 2. This way, the distance between most separated interacting sites can be held at 11 and 23 in the 4- and 8-chain systems, respectively. Since the exchange interactions run spatially throughout the system, the wave function converges very slowly with DMRG sweep but without getting trapped in a ‘false’ GS. We typically kept  $m \approx 1600 - 4000$  density-matrix eigenstates in the DMRG procedure. About 20 – 30 sweeps are necessary to obtain the GS energy within a convergence of  $10^{-7}|J_1|$  for each  $m$  value. All calculated quantities were extrapolated to  $m \rightarrow \infty$  and the maximum error in the GS energy is estimated as  $\Delta E/|J_1| \sim 10^{-4}$ , while the discarded weight in the renormalization is less than  $1 \times 10^{-6}$ . For high-spin states [ $S_{\text{tot}}^z \gtrsim (nL - 10)/2$ ] the GS energy can be obtained with an accuracy of  $\Delta E/|J_1| < 10^{-12}$  by carrying out several thousands sweeps even with  $m \approx 100 - 800$ . Then, we obtain the reduced saturation field  $h_s = g\mu_B H_s/|J_1|$  with high accuracy (e.g. 12 digits as compared to exact solutions available in some cases). The phase assignment in the 1D-diagrams shown in Refs. 7, 13–16 and in 3D (see Fig. 3) stems from an analysis of the magnetization curve just slightly below  $h_s$  as shown in Figs. 2 and 6. The signature of each region is the height of the magnetization

TABLE I: Saturation field  $h_s$  at  $\alpha = 0.332$ ,  $\beta_2 = 3/76$ , and  $\beta_1 = 0$ .  $J_{ic}$  has been multiplied by 4 for 2-chain systems.

$L$	single chain	2-chain system	8-chain system
16	0.0610480058942	0.315789473684	0.315789473684
48	0.0616910423378	0.315789473684	0.315789473684
96	0.0616910487270	0.315789473684	
144	0.0616910487247	0.315789473684	

steps  $\Delta S^z = 1, 2, 3, \dots$  for dipolar (1-magnon), quadrupolar (2-MBS), octupolar (3-MBS), and hexadecupolar (4-MBS), etc. phases, respectively. For the quadrupolar case the DMRG results are confirmed by the exact hard-core boson approach (HCBA) [11].

We start with the 1D problem. Using its frustration parameter  $\alpha = J_2/|J_1|$ , the critical point is given by the level crossing of a singlet and the highest multiplet state at  $\alpha_c = 1/4$ . Approaching  $\alpha_c$  from the spiral side  $\alpha \geq \alpha_c$ , it is clear that  $H_s^{1D}(\alpha)$  decreases and vanishes at  $\alpha_c \geq \alpha \geq 0$ . The curve  $H_s^{1D}(\alpha)$  is *not* smooth: it consists of quasi-linear parts with an infinite number of slope jumps at the endpoints of each quasi-linear part. These intervals become shorter and shorter when  $\alpha \rightarrow \alpha_c$  (see Fig. S3 of Ref. 7). These non-analytic endpoints reflect the changes of multi-MBS related low-energy excitations. This specific behavior persists also for  $D = 2, 3$  (see Figs. 4, 5) and is a signature of quantum phase transitions. Concerning  $\text{Li}_2\text{CuO}_2$  we stress that a 1D-approach yields for  $\alpha = 0.332$  [3],  $h_s = 0.0616916$  (see Table I) where  $g = 2$  and  $J_1 = 228$  K have been used. Thus, the empirical value  $H_s = 55.4$  T reported below is strongly *underestimated* by a 1D-approach. Hence, let us consider, what happens, if an IC of the type shown in Fig. 1 is switched on. In general, a complex phase diagram in terms of the IC and  $\alpha$  has been obtained (see Fig. 3 and Ref. 7). First, with increasing IC above a critical  $J_{ic}^{\text{cr},-}(\alpha)$  the MP

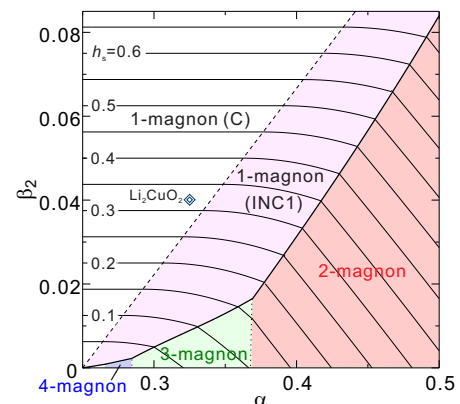


FIG. 3: (Color) Part of the 3D phase diagram around  $\text{Li}_2\text{CuO}_2$  in terms of  $\beta_2$  and  $\alpha$ .  $h_s$  is given by contour lines.

phase is removed in favor of one of the two incommensurate (INC) dipolar phases where  $H_s$  (given exactly by the SWT) is still affected by both in-chain and IC although the contribution of the former for  $\alpha < 0.54$  is significantly reduced as compared to the 1D case (see Figs. 4, 5). But at stronger IC for  $\alpha < 1$  one reaches a second critical point  $J_{ic,2}^{cr,+}$  where the INC phases are suppressed in favor of a commensurate (C) phase with FM in-chain correlations (see Figs. 3-5). Then  $H_s$  depends *solely* on the IC:

$$g\mu_B H_s = N_{ic} (J_{ic} + J'_{ic}) \text{ for } J_{ic} \geq J_{ic}^{cr,+}, \quad (1)$$

where  $N_{ic}$  is the number of nearest interchain neighbors (8 in case of  $\text{Li}_2\text{CuO}_2$ ). For  $\alpha > 1$  there is no C-phase. Now we take  $J'_{ic} = 0$  for the sake of simplicity. Taking into account it is possible but electronic structure calculations suggest  $J'_{ic}/J_{ic} \leq 0.1$ , only. Then,  $J_{ic}^{cr,+}(\alpha) = (4\alpha - 1)|J_1|/9$ , if  $\alpha < 0.57$  which is relevant for  $\text{Li}_2\text{CuO}_2$ . For the remaining interval  $0.57 \leq \alpha < 1$ , the INC2-C transition is of 1<sup>st</sup> order, see Ref. 7. Turning to  $\text{Li}_2\text{CuO}_2$  and ignoring a small anisotropy [3], we have

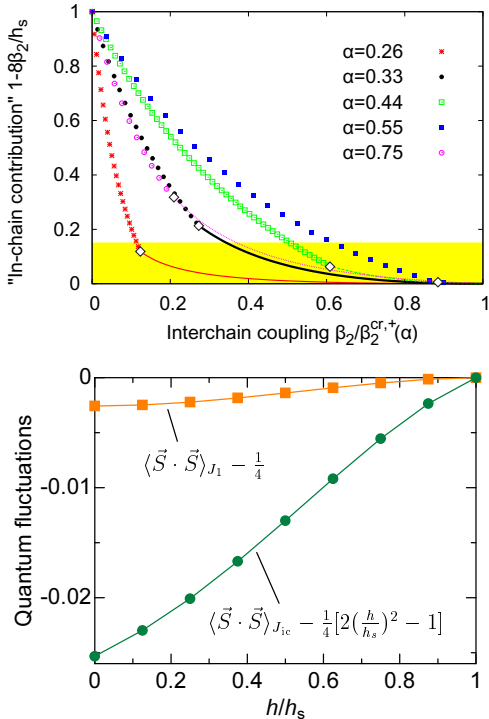


FIG. 4: (Color) Upper: Approximate relative in-chain contribution to the saturation field measured by its deviation from Eq. (1) for different  $\alpha$  values vs.  $\beta_2$  in units of its critical value  $\beta_2^{cr,+}$  (see Figs. 3, S1, and text). The yellow stripe highlights the region of predominant IC. The full line parts of a curve (below the symbol  $\diamond$ ) can be determined within the SWT, whereas the branches given by symbols are obtained by the DMRG and the HCBA methods. Lower: in-chain and IC spin-spin correlation functions vs. applied field, given by the filled symbols  $\blacksquare$  and  $\bullet$ , respectively, as obtained by DMRG.

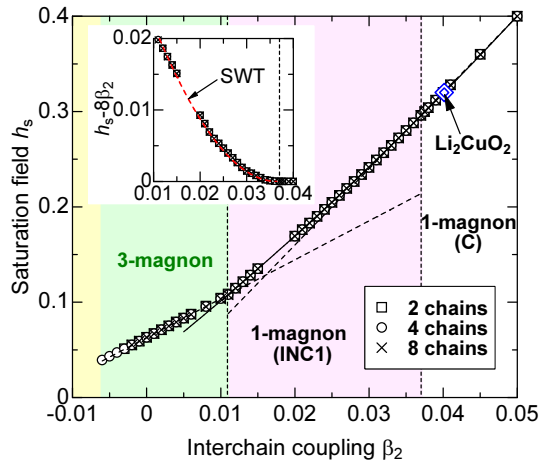


FIG. 5: (Color) The saturation field  $h_s$  at  $\alpha = 1/3$  vs.  $\beta_2$  from DMRG method. Notice the two critical IC values  $\beta_2^{cr,-} = J_{ic}^{cr,-}/|J_1| = 0.0109$  and  $\beta_2^{cr,+} = J_{ic}^{cr,+}/|J_1| = 0.03704$  denoted by dashed vertical lines. For INC1- and C-phases, see text. Inset: the weak non-linearity of  $h_s$  vs.  $\beta_2$ .

$J_{ic} \approx 9.04\text{K} > J_{ic}^{cr,+}(0.332) = 0.0364|J_1| \approx 8.2\text{K}$  [23]. Since in the C-phase  $H_s$  depends solely on  $J_{ic}$ , the IC can be directly read off from its measured value  $H_s = 55.4\text{T}$  yielding  $J_{ic} = 9.25\text{K}$  very close to  $9.04\text{K}$  from zero-field INS data [3]. In the INC1 phase  $J_{ic}$  dominates  $H_s$ . There above  $J_{ic}^{cr,-}(0.332) \approx 0.0109|J_1| = 2.49\text{K}$  only INC 1-magnon low-energy excitations exist. Below  $J_{ic}^{cr,-}$  3-MBS are recovered as low-energy excitations. The transition from the 3-MBS- to the INC1-phase is 1<sup>st</sup> order. The general situation is shown in Fig. 4. Well below  $J_{ic}^{cr,+}$  the saturation field significantly depends on  $\alpha$ . The yellow stripe highlights the region where the IC is predominant as addressed in our title. Here this dependence is weak and smooth. Subtracting their classical value, the spin-spin correlation functions show that the in-chain fluctuations vanish much faster than the IC ones for  $H \rightarrow H_s$  (see Fig. 4). This explains the surprising result of Eq. (1), too. For systems in the FM subcritical in-chain frustration regime  $\alpha < 1/4$  the in-chain contribution vanishes by definition. Hence, the external field has to overcome the AFM IC, only, and can be used to extract the IC exactly, if the corresponding  $g$ -factor is known (see Eq. (1)). This case is realized e.g. for  $\text{Ca}_2\text{Y}_2\text{Cu}_5\text{O}_{10}$  [25]. It has a similar IC geometry as  $\text{Li}_2\text{CuO}_2$ , but a 2D arrangement of chains, i.e.  $N_{ic} = 4$ . This reduced  $N_{ic}$  is overcompensated by a larger IC  $J_{ic} + J'_{ic} = 26\text{K}$  [26]. As a result we predict  $H_s \approx 61\text{T}$  and refine a recent overestimated value of  $70\text{T}$  from extrapolated low-field data [25].

Pulsed-field magnetization studies have been performed at the Dresden High Magnetic Field Laboratory in fields up to  $60\text{T}$ . The results taken at  $T = 1.45\text{K}$  for  $H \parallel b$ -axis on a  $\text{Li}_2\text{CuO}_2$  single crystal from the same batch as in the INS-study [3] is shown in Fig. 6. The data imply a quasi-linear increase of the magnetiza-

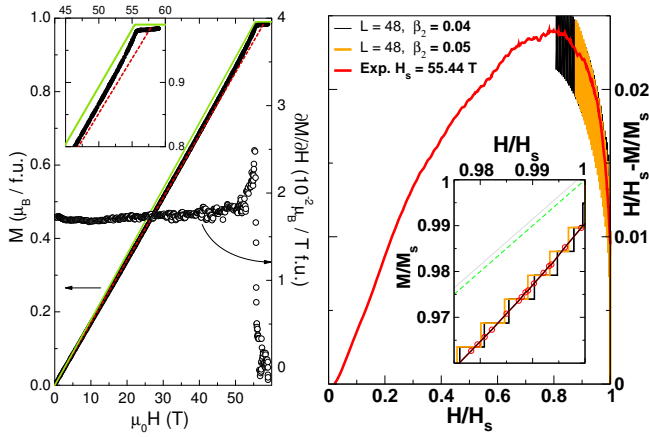


FIG. 6: (Color) Left: Magnetization  $M$  (left axis) and the derivative  $\partial M/\partial H$  ( $\circ$ ) from pulsed fields. Red (green dashed) line: auxiliary line to make the upturn near  $H_s$  better visible (classical curve (CC):  $M/M_s = H/H_s$ ). Right: Deviations from CC: DMRG vs. experiment for different IC  $\beta_2$  and a  $H_s$  value within the experimental error bars. Inset: Behavior just below  $H_s$  for the two  $\beta_2$ -values shown in the main part.

tion  $M(H)$  between 10 and 30 T, i.e.  $\partial M/\partial H = M' \approx \text{const.}$  Above about 50 T  $M'$  increases notably and pronounced peaks develop at  $55.4 \pm 0.25$  T and  $55.1 \pm 0.25$  T for two pieces of our single crystal. The sharp drop of  $M'$  towards 0 at higher fields justifies to attribute the peaks with  $H_s$ . The saturation moment amounts to  $M_s \approx 0.99 \pm 0.06 \mu_B/\text{f.u.}$  using  $g_b = 1.98 \pm 0.12$  in reasonable agreement with  $g_b = 2.047$  from low-field ESR-data at 300 K [24]. In Fig. 6 we compare  $M/M_s$  from the DMRG with the experiment for  $\text{Li}_2\text{CuO}_2$ . The DMRG description in this standard plot is rather good, but it is inconvenient to extract parameter values. This is due to the weak quantum fluctuations in  $\text{Li}_2\text{CuO}_2$ . The function  $f(M) = H/H_s - M/M_s$  reflects the remaining quantum fluctuations much better (see Fig. 6). Notice the enhanced fluctuations (i.e. smaller  $M(H)$ ) for the weaker IC (see inset). Noteworthy, the 'width' of the DMRG curves stems from the finite steps of  $M(H)$  due to the finite  $L$ . The almost straight shape of the  $M(H)$  curves shown in Figs. 2 and 6 evidences the 3D character of  $\text{Li}_2\text{CuO}_2$  in accordance with the large local magnetic moment  $\approx 0.93 \mu_B$  observed in the ordered phase at low  $T$  at  $h = 0$ . The measured  $H_s$  of our single crystal results in  $J_{\text{ic}} = 9.25 \pm 0.04$  K, close to the INS-data. Finally, we note that linear relations of two experimentally accessible thermodynamic quantities, the Curie-Weiss temperature and  $H_s$ , yield useful constraints for the in-chain  $J$ 's [7].

To summarize, the crucial role of AFM IC in frustrated quasi-1D systems, such as  $\text{Li}_2\text{CuO}_2$ , for their behavior in external fields and, particularly, the strength of  $H_s$  has been demonstrated. Extracting  $J_{\text{ic}}$  for that system from pulsed-field data, we arrived at 9.25 K, very close to a previous INS study which confirms the validity

of the adopted spin model. To extract  $J_{\text{ic}}$  a  $H_s$ -study is preferable over an INS, due its smaller error bars, the possibility to work with small single crystals and its much higher efficiency (concerning both time and costs). The large  $H_s$  from completely different studies discards any 1D scenario for  $\text{Li}_2\text{CuO}_2$ , even more,  $H_s$  itself is (within the isotropic model) independent of the in-chain couplings  $J_1$  and  $J_2$ . Thus, our results show *exactly* that for a relatively wide interval  $0 < \alpha < 1$  and collinear magnetic order at  $H = 0$ ,  $H_s$  depends only on the IC, irrespectively of its strength. A complete study of the entire phase diagram including the INC2-phase which at present is rather of academic interest, only, will be presented elsewhere. The MP-phases from 1D studies are very sensitive to the presence of IC in the 2D/3D counter parts. In particular, they can be readily eliminated by a weak AFM IC. Instead new incommensurate phases may occur. A study of other systems and their  $H_s$  within the approach proposed here is promising and in progress.

We thank the DFG (grants DR269/3-1, KL1824/2, RI615/16-1), PICS program (contr. CNRS 4767, NASU 267), EuroMagNET, & EU (contr. 228043) for support.

\* Corresponding author: s.l.drechsler@ifw-dresden.de

- 
- [1] A.W. Sandvik, Phys. Rev. Lett. **83**, 3069 (1999).
  - [2] S. Todo *et al.*, Phys. Rev. B **78** 224411 (2008).
  - [3] W.E.A. Lorenz *et al.*, EPL **88**, 37002 (2009).
  - [4] C. Yasuda *et al.*, Phys. Rev. Lett. **94**, 217201 (2005).
  - [5] S. Eggert, I. Affleck *et al.*, *ibid.* **89**, 047202 (2002).
  - [6] S.-L. Drechsler *et al.*, J. Mag. Mag. Mat. **316**, 306 (2007).
  - [7] See EPAPS Document No. [ ]. For more information on EPAPS, see <http://www.aip.org/pubservs/epaps.html>.
  - [8] A.V. Chubukov, Phys. Rev. B **44**, 4693 (1991).
  - [9] T. Vekua *et al.*, *ibid.* **76**, 174420 (2007).
  - [10] F. Heidrich-Meisner *et al.*, *ibid.* **74**, 020403R (2006).
  - [11] R.O. Kuzian and S.-L. Drechsler, *ibid.* **75**, 024401 (2007).
  - [12] M. Härtel *et al.*, *ibid.* **78**, 174412 (2008).
  - [13] D. Dmitriev and V. Krivnov, *ibid.* **79**, 054421 (2009).
  - [14] L. Kecke *et al.*, *ibid.* **76**, 060407 (2007).
  - [15] T. Hikihara *et al.*, *ibid.* **78**, 144404 (2008).
  - [16] J. Sudan, *et al.*, *ibid.* **80** 140402(R) (2009).
  - [17] R. Zinke, S.-L. Drechsler and J. Richter, *ibid.* **79**, 094425 (2009).
  - [18] H.T. Ueda and K. Totsuka, *ibid.* **80**, 014417 (2009).
  - [19] M. Zhitomirsky and H. Tsunetsugu, EPL **92**, 37001 (2010).
  - [20] L.E. Svistov *et al.*, Pis'ma v ZhETF **93**, 24 (2011).
  - [21] S.R. White, Phys. Rev. Lett. **69**, 2863 (1992).
  - [22] S. Qin *et al.*, Phys. Rev. B **52**, R5475 (1995).
  - [23] Considering the error bars of  $J_1$  and  $\alpha$ :  $\pm 5$  K and  $\pm 0.005$ , respectively, we see that  $J_{\text{ic}}^{\text{cr},+}$  is bounded by  $7.18 \text{ K} \leq J_{\text{ic}}^{\text{cr},+} \leq 8.54 \text{ K}$ , i.e.  $J_{\text{ic}}^{\text{cr},+}$  is certainly below  $J_{\text{ic}} = 9.04 \pm 0.1 \text{ K}$  (INS) or  $9.25 \pm 0.04 \text{ K}$  from our  $H_s$ -data.
  - [24] S. Kawamata, K. Okuda, and K. Kindo, J. Mag. Mag. Mat. **272-276**, 939 (2004).
  - [25] K. Kudo *et al.*, Phys. Rev. B **71**, 104413 (2005).
  - [26] M. Matsuda *et al.*, *ibid.* **63**, 180403 (2001).



**EPAPS supplementary online material:**  
**”Saturation field of frustrated chain cuprates: regions of predominant interchain coupling”**

S. Nishimoto<sup>1</sup>, S.-L. Drechsler<sup>1</sup>, R.O. Kuzian<sup>1</sup>, J. van den Brink<sup>1</sup>  
 J. Richter<sup>2</sup>, W.E.A. Lorenz<sup>1</sup>, Y. Skourski<sup>3</sup>, R. Klingeler<sup>4</sup>, B. Büchner<sup>1</sup>

<sup>1</sup>*IFW Dresden, P.O. Box 270116, D-01171 Dresden, Germany*

<sup>2</sup>*Universität Magdeburg, Institut für Theoretische Physik, Germany*

<sup>3</sup>*Hochfeld-Magnetlabor Dresden, Helmholtz-Zentrum Dresden-Rossendorf, D-01314 Dresden, Germany*

<sup>4</sup>*Kirchhoff Institute for Physics, University of Heidelberg, D-69120 Heidelberg, Germany*

In the present Supplementary part we provide the reader with the general phase diagram of the 3D model with a diagonal antiferromagnetic (AFM) interchain coupling (IC)  $J_{ic}$  that couples each site in a frustrated  $J_1$ - $J_2$  single chain to its next-nearest-neighbor (NNN) sites in the adjacent chains. This type of IC is realized in  $\text{Li}_2\text{CuO}_2$ , see Fig. 1 of the main text. Its rigorous treatment leads for the incommensurate parts INC1 and INC2 of the general phase diagram (see Fig. S1) to somewhat tedious analytical expressions for the saturation field  $H_s$  provided here for an interested reader explicitly. Then, in the spirit of our proposed efficient thermodynamic approach, we present simple but exact equations where  $H_s$  together with the Curie-Weiss temperature can be used to get insight into the microscopic exchange couplings. Finally, we present DMRG data mentioned in main text for the most realistic case of a very weak nearest-neighbor (NN) IC  $\beta_1 = J'_{ic}/|J_1|$  and a predominant NNN IC  $\beta_2 = J_{ic}/|J_1|$  with parameters relevant for  $\text{Li}_2\text{CuO}_2$  suggested by band structure calculations [1].

### PHASE DIAGRAMS AND THE DETERMINATION OF THE SATURATION FIELD

We start with the presentation of the whole phase diagram [2], see Fig. S1.

Let us first remind the behavior of the saturation field at the basis line of the general 3D phase diagram, i.e. the 1D limit of the considered problem, see Fig. S2 and also Refs. 15 and 16 in the main text. At present the higher multipolar phases beyond the four-magnon sector near the critical point  $\alpha_c = 1/4$  cannot be assigned numerically with sufficient precision as a sequence of 5-, 6-, etc. phases as suggested by Krivnov and Dmitriev on general grounds [3]. The question mark in Fig. S2 reminds the reader of this numerically still somewhat unclear situation.

The hard-core boson approach provides an exact solution (see e.g. Ref. 11 in the main text) for the 2-magnon (nematic, quadrupolar (QP)) phase. In the 1D case we obtain in the QP phase

$$h_s = 2\alpha - 1 + 0.5/(\alpha + 1), \quad (\text{S1})$$

valid above a *critical* point  $\alpha_3 \approx 0.3676776$ , i.e. for  $\alpha \geq \alpha_3$ . Below  $\alpha_3$  at first 3-MBS and then 4-MBS, etc. occur as the lowest excitations. In the 1D case our DMRG data for the 3-magnon (octupolar) phase can be described with high precision by an expansion up to the second order around the critical point  $\alpha_3$

$$h_s^{3M}(\alpha) = h_{03} + h'_3(\alpha - \alpha_3) + 0.5h''_3(\alpha - \alpha_3)^2 + \dots, \quad (\text{S2})$$

where  $h_{03} = 0.1009384$ ,  $h'_3 = 1.1511$ , and  $h''_3 = 2.95699$ . Eq. (S2) is valid for  $\alpha_3 \geq \alpha \geq \alpha_4 \approx 0.284533$ . A similar simple but semi-analytic solution, only, can be derived also for the 4-magnon phases based on a fit of our DMRG results.

The inspection of Fig. S3 shows that in the limiting case  $\alpha = 1$  at sizable IC, say for  $J_{ic}/J_2 \geq 1/3$ , the saturation field  $H_s$  is also dominated by the IC. Note that a similar effect for a sizable IC appears also for  $\alpha > 1$ . But it becomes weaker with increasing  $\alpha$ .

### THE 3D SPIN-HAMILTONIAN

The spin-1/2 Heisenberg Hamiltonian reads

$$\hat{H}_H = \sum_{\mathbf{R}} \left[ J_1 (\hat{\mathbf{S}}_{\mathbf{R}} \cdot \hat{\mathbf{S}}_{\mathbf{R}+\mathbf{b}}) + J_2 (\hat{\mathbf{S}}_{\mathbf{R}} \cdot \hat{\mathbf{S}}_{\mathbf{R}+2\mathbf{b}}) + J_{ic} \sum_{\mathbf{r}} (\hat{\mathbf{S}}_{\mathbf{R}} \cdot \hat{\mathbf{S}}_{\mathbf{R}+\mathbf{r}}) + J'_{ic} \sum_{\mathbf{r}'} (\hat{\mathbf{S}}_{\mathbf{R}} \cdot \hat{\mathbf{S}}_{\mathbf{R}+\mathbf{r}'}) - \mu (\mathbf{H} \cdot \hat{\mathbf{S}}_{\mathbf{R}}) \right], \quad (\text{S3})$$

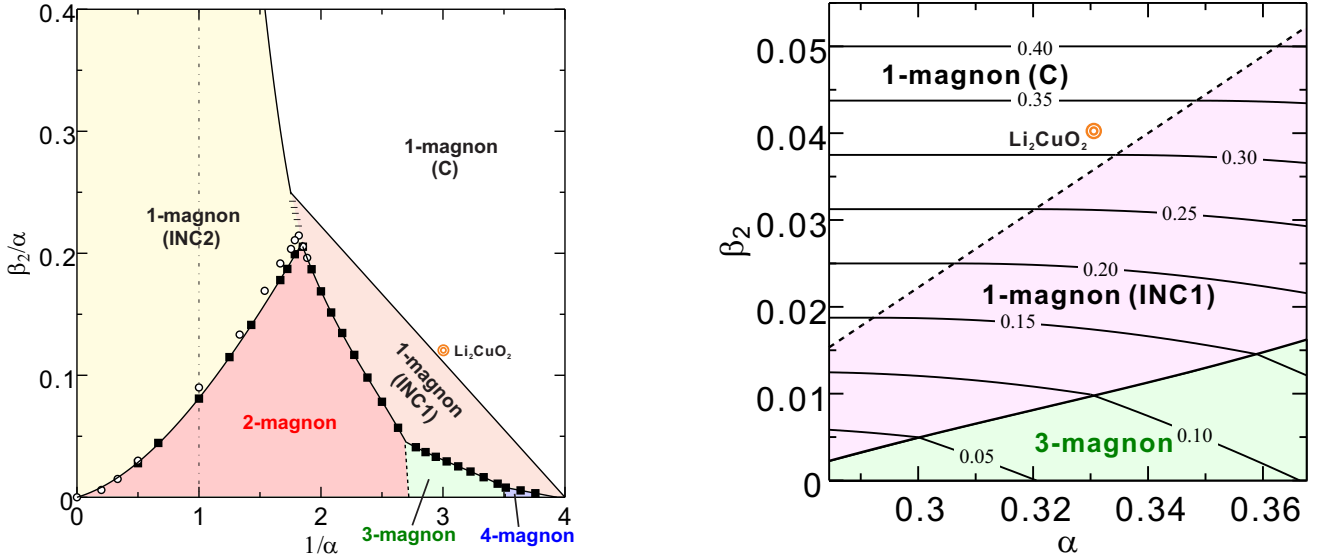


FIG. S1: (Color) Left: General phase diagram for frustrated chains with an AFM IC  $\beta_2$  of the diagonal type as realized in  $\text{Li}_2\text{CuO}_2$  (see Figs. 1 and 3 of the main text) but for arbitrary reciprocal frustration parameter  $1/\alpha = |J_1|/|J_2|$ . The symbol  $\blacksquare$  denotes our DMRG results and the symbol  $\circ$  stands for the exact hard-core boson approach. Notice a second incommensurate phase INC2. Its border line to the commensurate (C) phase approaches asymptotically the value of  $1/\alpha = 1$  as shown by the dashed vertical line. For the behavior along the basis line, i.e. the 1D limit, see Fig. S2 and Refs. 15 and 16 in the main text. The line separating the two incommensurate one-magnon phases INC1 and INC2 represents a first-order transition. Right: Enlarged contour plot of the dimensionless saturation field  $h_s = g\mu_B H_s/|J_1|$  vs. the in-chain frustration rate  $\alpha$  and the interchain interaction  $\beta_2$  in the vicinity of parameters for  $\text{Li}_2\text{CuO}_2$ . The boundary between the INC1 and the 3-magnon phases is obtained by our DMRG calculations. Notice the slightly non-equidistant height differences in the contour lines of constant  $h_s$  in the INC1 region as compared to equidistant ones in the C-region as well as the changed axis notation as compared with the left part.

where  $\mathbf{R}$  is the position vector of a Cu site in the lattice,  $\mathbf{r} = (\mathbf{3b} \pm \mathbf{a} \pm \mathbf{c})/2$ ,  $\mathbf{r}' = (\mathbf{b} \pm \mathbf{a} \pm \mathbf{c})/2$   $\mathbf{a}, \mathbf{b}, \mathbf{c}$  are lattice vectors.

The one- and two-magnon excitation spectrum for magnetic fields  $H > H_s$  can be found *exactly* at  $T = 0$ . The classical fully spin-polarized ground state is also an exact eigenstate of the quantum Hamiltonian. The spin-deviation (magnon) operators for the spin-1/2 Heisenberg Hamiltonian are Pauli (hard-core boson) operators, in terms of which the Hamiltonian is rewritten as [4]

$$\hat{H} = \hat{H}_0 + \hat{H}_{\text{int}}, \quad (\text{S4})$$

$$\hat{H}_0 = \sum_{\mathbf{R}} \left[ \omega_0 \hat{n}_{\mathbf{R}} + J_1 b_{\mathbf{R}}^\dagger b_{\mathbf{R}+\mathbf{b}} + J_2 b_{\mathbf{R}}^\dagger b_{\mathbf{R}+2\mathbf{b}} + J_{\text{ic}} \sum_{\mathbf{r}} b_{\mathbf{R}}^\dagger b_{\mathbf{R}+\mathbf{r}} + J'_{\text{ic}} \sum_{\mathbf{r}'} b_{\mathbf{R}}^\dagger b_{\mathbf{R}+\mathbf{r}'} \right], \quad (\text{S5})$$

$$\omega_0 \equiv \mu H - [J_1 + J_2 + 4(J_{\text{ic}} + J'_{\text{ic}})], \quad \hat{n}_{\mathbf{R}} \equiv b_{\mathbf{R}}^\dagger b_{\mathbf{R}}$$

$$\hat{H}_{\text{int}} = \sum_{\mathbf{R}} \left[ J_1 \hat{n}_{\mathbf{R}} \hat{n}_{\mathbf{R}+\mathbf{b}} + J_2 \hat{n}_{\mathbf{R}} \hat{n}_{\mathbf{R}+2\mathbf{b}} + J_{\text{ic}} \sum_{\mathbf{r}} \hat{n}_{\mathbf{R}} \hat{n}_{\mathbf{R}+\mathbf{r}} + J'_{\text{ic}} \sum_{\mathbf{r}'} \hat{n}_{\mathbf{R}} \hat{n}_{\mathbf{R}+\mathbf{r}'} \right], \quad (\text{S6})$$

where  $\mu = g\mu_B$  and the  $z$ -axis is parallel to  $\mathbf{H}$ . The transverse part of the Heisenberg Hamiltonian  $\hat{H}$  (S3) defines the one-particle hoppings in  $\hat{H}_0$  (S5), the Ising part contributes the interaction (S6) and the on-site energy value  $\omega_0$ . Note that a negative (ferromagnetic) exchange in (S6) acts as an attraction between the magnons. In 1D  $J_1$ - $J_2$ -chains with  $J_1 < 0$  and  $J_2 > 0$  this leads always to the formation of multimagnon bound-states. In 2D and 3D lattices the bound-states formation is possible only if the attraction overcomes the kinetic energy. Besides on the strength of the AFM interchain interaction it depends also on the number of available interchain neighbors which in the case of diagonal IC is doubled as compared with the frequently studied but much simpler case of perpendicular IC of unshifted chains (see Figs. 1 of the main text and of Ref. 17 therein). Therefore, the case of a 3D chain arrangement as in  $\text{Li}_2\text{CuO}_2$  is especially effective in deconfining the multimagnon bound states and suppressing a spiral type 1-magnon state as the phase INC1 and INC2 considered above.

The Hamiltonian (S4) conserves the number of magnons. So, the excitation spectrum may be found separately for

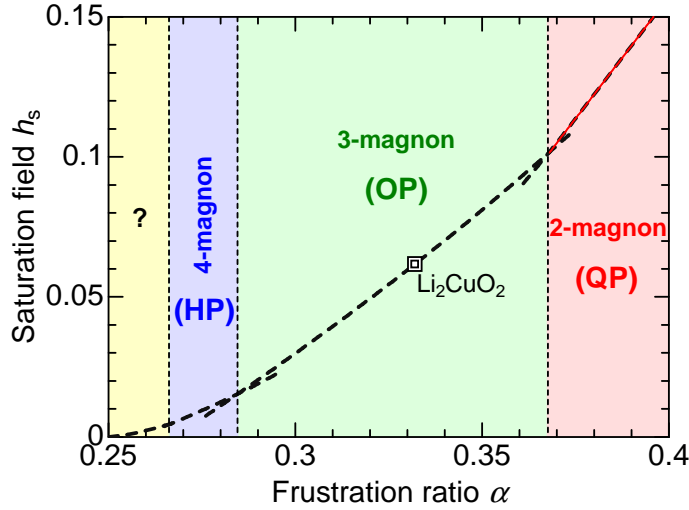


FIG. S2: (Color) Saturation field  $h_s$  vs. frustration ratio  $\alpha$  of a single chain according to our DMRG. Notice the change in the slope indicated by the vertical dashed lines. The octupolar (OP or 3-MBS) is realized for  $0.2845 \leq \alpha \leq 0.3676$  in between the hexadecupolar (HP or 4-MBS) and the quadrupolar (QP or 2-MBS) regions. Dashed line: DMRG results (each dash contains about 5 data points). Red solid line: Analytical curve from the exact 2-magnon solution obtained from the hard-core boson representation of the general spin Hamiltonian (valid exactly in the one- and two-magnon regions) given in Eq. (S1). The question mark in the most left yellow region close to the critical point  $\alpha = 1/4$  stands for numerically still unresolved but expected higher order multipolar phases (see text).

one-, two-, three- etc. magnon sectors of the Hilbert space. The saturation field is determined by the condition of the stability of the ground state. It becomes unstable when the frequency of a certain excitation vanishes.

## THE TWO INCOMMENSURATE ONE-MAGNON PHASES INC1 AND INC2

The energy of one-particle (1-magnon) excitations is particularly simple. For the isotropic model and  $J'_{ic} = 0$  it reads

$$\omega_{\mathbf{q},\sigma} = \mu_B H_s + J_1 (\cos q_b - 1) + J_2 (\cos 2q_b - 1) + 4J_{ic} \left( \sigma \cos \frac{q_a}{2} \cos \frac{3q_b}{2} \cos \frac{q_c}{2} - 1 \right), \quad (\text{S7})$$

where we have retained the AFM Brillouin zone,  $\sigma \equiv \pm 1$  enumerates the two branches of the spectrum. The extrema of the one-particle spectrum are given by the equation  $\nabla \omega_{\mathbf{q}} = 0$ , which gives for our model  $q_a = q_c = 0$ , and

$$\sin \frac{q_b}{2} \left[ J_1 \cos \frac{q_b}{2} + 4J_2 \left( 2 \cos^3 \frac{q_b}{2} - \cos \frac{q_b}{2} \right) + 3\sigma J_{ic} \left( 4 \cos^2 \frac{q_b}{2} - 1 \right) \right] = 0. \quad (\text{S8})$$

The extrema for the two branches occur at  $q_{b,\sigma} = 0$  and at incommensurate values of  $q_b = q_{i,\sigma}$ ,  $i = 1, 2, 3$ , where the expression in square brackets vanishes

$$\cos \frac{q_{i,\sigma}}{2} = y_{i,\sigma} - \sigma \frac{J_{ic}}{2J_2},$$

where  $y$  is the root of the cubic equation

$$y_{1,\sigma} = 2\sqrt{-\frac{p}{3}} \cos \frac{\gamma_\sigma}{3}, \quad y_{2,3,\sigma} = -2\sqrt{-\frac{p}{3}} \cos \frac{\gamma_\sigma \pm \pi}{3} \quad (\text{S9})$$

$$\cos \gamma_\sigma \equiv -\frac{\sigma q}{2\sqrt{(-p/3)^3}}, \quad (\text{S10})$$

$$p \equiv -\frac{1}{2} \left[ 1 - \frac{J_1}{4J_2} + \frac{3J_{ic}^2}{2J_2^2} \right], \quad (\text{S11})$$

$$q \equiv -\frac{J_{ic}}{2J_2} \left[ p + \frac{1}{4} \left( \frac{J_{ic}}{J_2} \right)^2 + \frac{3}{4} \right]. \quad (\text{S12})$$

In the dipolar phase, the saturation field  $H_s$  is determined by the condition that the energy of the lowest one-magnon excitation  $\omega_{\mathbf{q},\min}$  vanishes. Then, from Eq. (S7) the dimensionless saturation field  $h_s = g\mu_B H_s / |J_1|$  is determined by the equation

$$h_s = (\cos q_{b,\min} - 1) - \alpha (\cos 2q_{b,\min} - 1) - 4\beta \left( \sigma \cos \frac{3q_{b,\min}}{2} - 1 \right). \quad (\text{S13})$$

For an isolated chain ( $\beta_2 = 0$ ) the two branches are degenerated and both reach the minimum at  $q_0(0) = \arccos(1/4\alpha)$ . For finite  $J_{ic}$  and  $\alpha \lesssim 0.57$  (the INC1 phase) the minimum occurs at  $q_{1,-1}$  of the branch  $\sigma = -1$ . With the increase of  $\beta_2$  the minimum shifts towards the centrum of BZ, which is reached at  $\beta_2 = \beta_2^{\text{cr}}(\alpha) = (4\alpha - 1)/9$ .

Now we note that  $0 < \beta_2 \leq \beta_2^{\text{cr}} \leq 4/9$  holds for all frustration values  $1/4 \leq \alpha < 0.57$ . Then the expression (S13) may be expanded in powers of  $\beta_2^{\text{cr}} - \beta_2$

$$h_s(\alpha, \beta_2) = 8\beta_2 - \frac{7776(1-20\alpha)(\beta_2^{\text{cr}} - \beta_2)^2}{a^2} \left[ h_0 + h_1(\beta_2^{\text{cr}} - \beta_2) + h_2(\beta_2^{\text{cr}} - \beta_2)^2 \right], \quad (\text{S14})$$

$$a \equiv 5 - 72\alpha + 1744\alpha^2,$$

$$h_0 \equiv \frac{1}{2} (5 - 72\alpha + 592\alpha^2), \quad (\text{S15})$$

$$h_1 \equiv \frac{18(7 - 84\alpha + 1184\alpha^2)(1 - 20\alpha)}{a}, \quad (\text{S16})$$

$$h_2 \equiv \frac{324(5 - 45\alpha + 1204\alpha^2)(1 - 20\alpha)^2}{a^2}. \quad (\text{S17})$$

For  $\beta_2 > \beta_2^{\text{cr}}$  the minimum persists at  $q_{b,-1} = 0$ , and the saturation field is simply given by  $h_s = N_{ic}\beta_2 = 8\beta_2$ . For  $\text{Li}_2\text{CuO}_2$  one has  $\beta_2 \approx 3/76 \approx 0.03947 > \beta_2^{\text{cr}} = 0.0364$ . For  $0.57 < \alpha < 1$  the minimum occurs at  $q_{1,+1}$  of the branch  $\sigma = +1$  for  $\beta$  smaller a certain value  $\beta_2^{\text{cr}}(\alpha) > (4\alpha - 1)/9$  where it jumps at  $q_{b,-1} = 0$ . So, for this range of the frustration ratio  $\alpha$ , the transition between the commensurate C-phase with FM in-chain ordering and the new incommensurate INC2 phase is of first order. The corresponding phase boundary may be found from the condition  $\omega_{+1}(q_{1,+1}) = \omega_{-1}(0)$ , and it is given by the following parametric function

$$\alpha(t) = \frac{1 - t + \frac{2(t-2)(2t-1)}{2t-7}}{4t \left[ t(t-1) + \frac{2(2t-1)^2}{2t-7} \right]}, \quad (\text{S18})$$

$$\beta_2^{\text{cr}}(t) = \frac{4t\alpha(t)(2t-1) + t-2}{(2t-7)(2t-1)}. \quad (\text{S19})$$

Finally, for  $\alpha \geq 1$  the minimum resides at  $q_{1,+1}$  for all values of IC. The resulting phase diagram is shown schematically in Fig. S1 (left).

## EXACT THERMODYNAMIC CONSTRAINTS INVOLVING THE SATURATION FIELD

To demonstrate the general applicability of our proposed efficient thermodynamic method to extract exchange integrals from simple and "cheap" measurements, we present a collection of simple but rigorous constraints valid for situations where to first approximation a chain-like compound can be described by the adopted isotropic  $J_1$ - $J_2$ -model for a single chain with one main interchain coupling, only, but with various geometries of the chain arrangement. Generalizations to several interchain couplings and to models with spin anisotropy are straightforward and will be given elsewhere.

With the experimental Curie-Weiss temperature  $\Theta_{\text{CW}}$  (that governs the high- $T$  spin susceptibility  $\chi(T) \sim 1/(T - \Theta_{\text{CW}})$ ) which is simply related to the Hamiltonian parameters by

$$\Theta_{\text{CW}} \approx -0.5 [J_1 + J_2 + 0.5N_{ic}(J_{ic} + J'_{ic})] \quad (\text{S20})$$

the whole set of interchain couplings between NN chains, including in particular  $J_{ic}$  as well as all (weak) additional terms such as  $J'_{ic}$  etc. can be replaced by  $\Theta_{\text{CW}}$  and Eq. (1) of the main text. As a results the we find a useful empirical constraint for the in-chain exchange couplings  $J_1$  and  $J_2$ .

$$g\mu_B H_s + 4\Theta_{\text{CW}} = 2|J_1|(1 - \alpha). \quad (\text{S21})$$



Using the experimentally measured saturation field for  $\text{Li}_2\text{CuO}_2$  of about 55.4 T as reported in the main text, we predict a ferromagnetic Curie-Weiss temperature of about 55 K to be derived from high temperature ( $T > 400$  K) susceptibility measurements not yet performed. For a strictly perpendicular NN IC, only, (see e.g. Fig. 1 in Ref. 17) the strong influence of the interchain coupling on the in-chain ordering is much reduced and as a result the 3D(2D) C-phase is missing, i.e. there is only one critical IC separating the *single* INC phase from the MP phases. In particular, the two-magnon phase shows a round maximum [5, 6] in the 3D case near  $1/\alpha = 0.906$  instead of the cusp seen in figure S1 (left) near  $1/\alpha = 1.754$ . In the neighboring single INC-phase  $h_s$  reads

$$h_s = 2\alpha - 1 + 0.125/\alpha + N_{\text{ic}}J_{\text{ic}}, \quad (\text{S22})$$

where  $N_{\text{ic}}=2$  (4) for a 2D (3D) chain arrangement, respectively. Then Eq. (S21) is replaced by

$$g\mu_{\text{B}}H_s + 4\Theta_{\text{CW}} = |J_1| [1 + 0.125/\alpha] . \quad (\text{S23})$$

In the two magnon-phase for weak IC one has

$$g\mu_{\text{B}}H_s + 2\Theta_{\text{CW}} = |J_1| [\alpha + 0.5/(1 + \alpha)] \quad (\text{S24})$$

(note the new prefactor of 2 in front of  $\Theta_{\text{CW}}$ ). Similar simple constraints can be derived for any type of interchain couplings. They provide another part for the proposed thermodynamic approach to extract microscopic exchange integrals from few experimental numbers, only, instead to fit for instance approximate expressions for complex quantities such as the susceptibility or the magnetic specific heat in more or less extended wide temperature intervals.

## SOME DETAILED DMRG AND HARD-CORE BOSON RESULTS

Finally, we present numerical DMRG data to demonstrate the extremely fast convergence with respect to the number of chains taken into account. Notice that here also a weak NN interchain coupling  $\beta_1$  has been taken into account. The DMRG result is very close to the analytical result of 0.350877192982456 given by Eq. (1) in the main text.

TABLE S1: Saturation field  $h_s$  at  $J_1 = -1$ ,  $\alpha = 0.332$ ,  $\beta_2 = 3/76$ ,  $\beta_1 = 1/228$ .  $\beta_2$  and  $\beta_1$  are multiplied by four and two for 2-chain and 4-chain clusters, respectively.

$L$	single chain	2-chain cluster	4-chain cluster	8-chain cluster
16	0.0610480058942	0.350877192884	0.350877192884	0.350877192884
20	0.0618650864275	0.350877192884	0.350877192884	0.350877192884
24	0.0616475064797	0.350877192884	0.350877192884	0.350877192884
28	0.0617013393558	0.350877192884	0.350877192884	0.350877192884
32	0.0616885713591	0.350877192884	0.350877192884	0.350877192884
36	0.0616916345343	0.350877192884	0.350877192884	0.350877192884
40	0.0616909145148	0.350877192884	0.350877192884	0.350877192884
44	0.0616910784629	0.350877192884	0.350877192884	0.350877192884
48	0.0616910423378	0.350877192884	0.350877192884	0.350877192884
96	0.0616910487270	0.350877192884		
144	0.0616910487247	0.350877192884		

In order to illustrate another aspect of the accuracy of our DMRG calculations, we briefly discuss the difficult gap problem at  $H = 0$  of a single frustrated chain with a FM  $J_1$  raised by recent field theory approaches [7–9]. These theories predict a gap  $\Delta$  of unknown magnitude. Since at present there are no hints from numerical studies for such a behavior, it is generally accepted that such a gap should be very small [9]. According to our DMRG calculations we estimate  $10^{-5}|J_1|$  as an upper bound. For the case of  $\text{Li}_2\text{CuO}_2$  under consideration this corresponds to 0.01 to 0.02 K, only. Anyhow, such a tiny gap, if it at all exists, would be of academic interest, only.

Now we present some numerical results from exact relations obtained in the hard-core boson approach. In Fig. S3 several examples for the IC dependence of the saturation field  $h_s$  are presented. Similar dependencies are obtained for arbitrarily large in-chain frustration ratios  $\alpha$ . In the 3D case with a finite antiferromagnetic  $J_{\text{ic}}$  the saturation field  $h_s$  is always affected by the former in contrast to the in-chain coupling which can drop out exactly what happens in the commensurate C-phase.

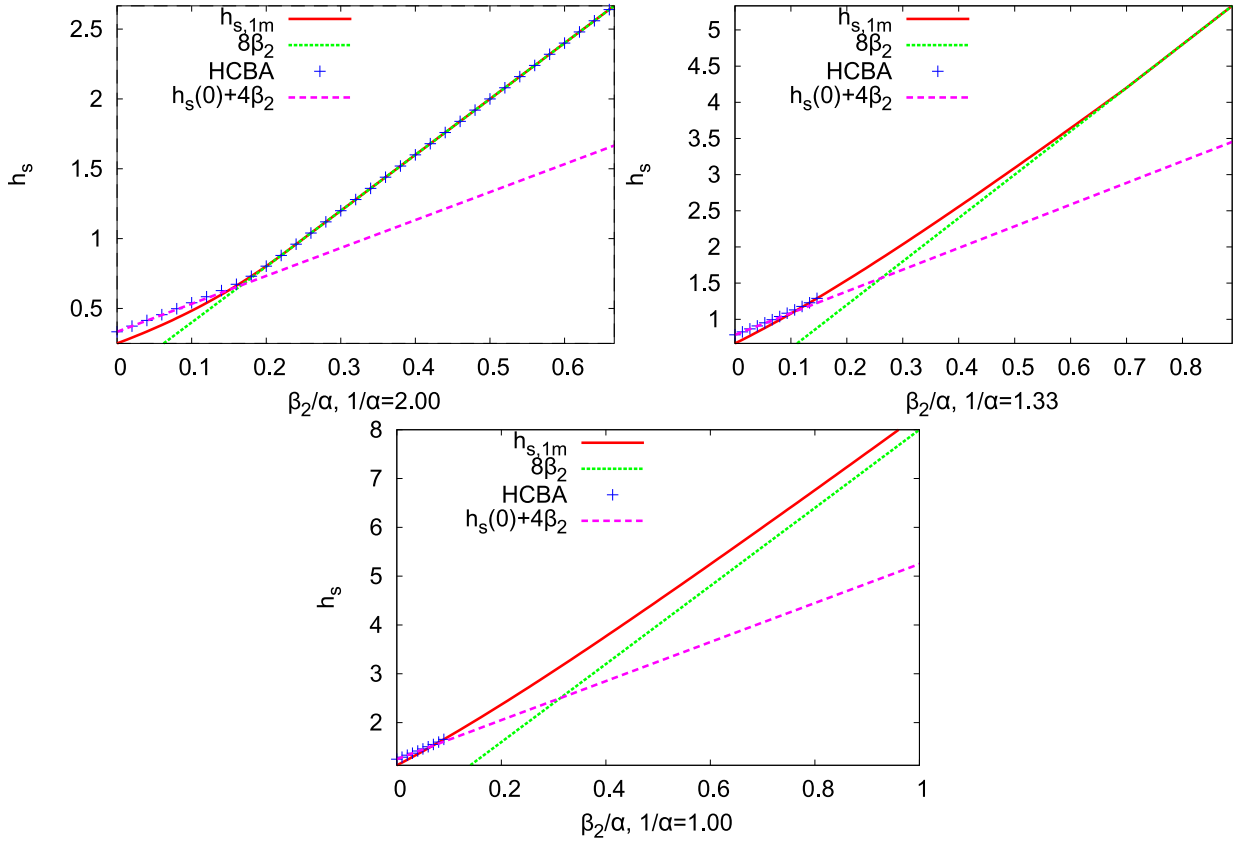


FIG. S3: (Color) Saturation field for different in-chain frustration rates  $\alpha = 0.5, 0.75,$  and  $1.0$  vs. IC  $\beta_2/\alpha = J_{ic}/J_2$ . The results of the exact hard-core boson approach are shown by symbols; the red solid line shows the one-magnon result, which becomes exact for  $\beta_2 > \beta_2^{cr,-} = J_{ic}^{cr,-}/|J_1|$  as explained in the main text (see also Figs. 3-5, therein). The green dashed line shows the value, which is reached in the commensurate C-phase, where the dependence on  $J_1, J_2$  vanishes identically; the magenta thin line shows an approximation to the exact solution in the 2-magnon phase.

- 
- [1] U. Nitzsche *et al.* to be published.
  - [2] The actual numerical reasons for the rather small deviations between the DMRG results and those of the hard-core boson approach will be discussed in more detail elsewhere.
  - [3] D.V. Dmitriev, V.Ya. Krivnov, Phys. Rev. B **73**, 024402 (2006).
  - [4] S.V. Tyablikov, *Methods in the Quantum Theory of Magnetism* (Plenum, New York, 1967).
  - [5] S. Nishimoto, S.-L. Drechsler, R. Kuzian, J. Richter, and J. van den Brink, "Quasi-1d quantum helimagnets: The fate of multipolar phases", arXiv:1005.5500 and to be published.
  - [6] T.K. Ueda and K. Totsuko, Phys. Rev. B **80**, 014417 (2010).
  - [7] A.A. Nersesyan, A.O. Gogolin, and F.H.L. Eßler, Phys. Rev. Lett. **81**, 910 (1998).
  - [8] C. Itoi and S. Qin, Phys. Rev. B **63**, 224423 (2001).
  - [9] E. Berg, T.H. Geballe, and S.A. Kivelson, Phys. Rev. B **76**, 214505 (2007).
-